

The UV properties of E+A galaxies: constraints on feedback-driven quenching of star formation

S. Kaviraj¹, L. A. Kirkby¹, J. Silk¹ and M. Sarzi²

¹*Department of Physics, University of Oxford, Keble Road, Oxford OX1 3RH, UK*

²*Centre for Astrophysics Research, University of Hertfordshire, Hatfield, AL10 9AB, UK*

29 May 2007

ABSTRACT

We present the first large-scale study of E+A galaxies that incorporates photometry in the ultraviolet (*UV*) wavelengths. E+A galaxies are ‘post-starburst’ systems, with strong Balmer absorption lines indicating significant recent star formation, but without [OII] and H α emission lines which are characteristic of ongoing star formation. The starburst that creates the E+A galaxy typically takes place within the last Gyr and creates a high fraction (20-60 percent) of the stellar mass in the remnant over a short timescale (< 0.1 Gyrs). We find a tight correlation between the luminosity of our E+A galaxies and the implied star formation rate (SFR) during the starburst. While low-luminosity E+As ($M(z) > -20$) exhibit implied SFRs of less than $50 M_{\odot} yr^{-1}$, their luminous counterparts ($M(z) < -22$) shows SFRs greater than 300 and as high as $2000 M_{\odot} yr^{-1}$, suggesting that luminous and ultra-luminous infrared galaxies in the low-redshift Universe could be the progenitors of massive nearby E+A galaxies. We perform a comprehensive study of the characteristics of the quenching that truncates the starburst in E+A systems. We find that, for galaxies less massive than $10^{10} M_{\odot}$, the *quenching efficiency* decreases as the galaxy mass increases. However, for galaxies more massive than $10^{10} M_{\odot}$, this trend is reversed and the quenching efficiency increases with galaxy mass. Noting that the mass threshold at which this reversal occurs is in excellent agreement with the mass above which AGN become significantly more abundant in nearby galaxies, we use simple energetic arguments to show that the bimodal behaviour of the quenching efficiency is consistent with AGN and supernovae (SN) being the principal sources of negative feedback above and below $M \sim 10^{10} M_{\odot}$ respectively. The arguments assume that quenching occurs through the mechanical ejection or dispersal of the gas reservoir and that, in the high mass regime ($M > 10^{10} M_{\odot}$), the Eddington ratios in this sample of galaxies scale as M^{γ} , where $1 < \gamma < 3$. Finally, we use our E+A sample to estimate the time it takes for galaxies to migrate from the blue cloud to the red sequence. We find migration times between 1 and 5 Gyrs, with a median value of 1.5 Gyrs.

Key words: galaxies: elliptical and lenticular, cD – galaxies: evolution – galaxies: formation – galaxies: fundamental parameters

1 INTRODUCTION

‘E+A’ galaxies exhibit strong Balmer absorption lines, characteristic of significant recent star formation, but lack [OII] or H α emission which are characteristic of ongoing star formation. Their spectral features indicate that a vigorous episode of recent star formation in these systems has been quenched abruptly. As ‘post-starburst’ systems, E+A galaxies provide a valuable evolutionary link between the gas-rich star-forming population and gas-poor quiescent sys-

tems. The persistent dichotomy in galaxy colours over a large range in redshift, coupled with the gradual build-up of the red sequence over time (e.g. Bell et al. 2004), indicates that *how* and *over what timescale* galaxies evolve from the ‘blue cloud’ to the ‘red sequence’ is of significant importance in understanding the macroscopic evolution of the galaxy population over the lifetime of the Universe. The characteristics of E+A galaxies provide a unique (but transient!) window into the very point where this transition from blue-cloud to red sequence is about to begin. Understanding what drives their vigorous star formation episode and, in particu-

* E-mail: skaviraj@astro.ox.ac.uk

lar, what causes it to be quenched so suddenly is clearly an important step in our understanding of galaxy evolution.

First noticed by Dressler & Gunn (1983) in distant ($z \sim 0.4$) clusters, E+A galaxies have been subsequently found to be abundant in all types of environments. At intermediate redshifts ($0.3 < z < 1$), the proportion of E+A galaxies appears to be a factor of four greater in clusters than in the field (Tran et al. 2004). In the nearby Universe E+A galaxies have been detected mainly in the field (Zabludoff et al. 1996; Quintero et al. 2004) primarily because most galaxies do not reside in dense cluster-like environments. Indeed, the overall distribution of the local environments of E+A systems follows that of the general galaxy population as a whole (Blake et al. 2004). The fraction of E+A systems in clusters shows a rapid decline from intermediate redshifts ($z \sim 0.5$) where it is typically higher than 20 percent (e.g. Couch & Sharples 1987; Belloni et al. 1995) to less than 1 percent in local clusters (Fabricant et al. 1991).

Several plausible explanations for the E+A phenomenon have been proposed and studies indicate that there are multiple channels for creating such post-starburst spectral signatures. Since E+A galaxies were first detected in clusters, it was initially thought that their production required a cluster-specific mechanism, such as galaxy harassment or ram-pressure stripping. However, their abundant presence in the field indicates that other channels exist for the production of E+A systems (e.g. Goto 2005), although cluster-specific mechanisms may contribute or even dominate their evolutionary pathways in dense regions of the Universe.

Another possible explanation for E+A-like spectra is that the optical emission lines are heavily suppressed by dust obscuration (e.g. Smail et al. 1999; Couch & Sharples 1987; Poggianti & Wu 2000). An efficient test of this scenario is to observe the E+A population in the radio wavelengths where the effects of dust obscuration are absent. However, a radio study of 15 galaxies in the Zabludoff et al. (1996) sample by Miller & Owen (2001) detected only two at radio luminosities which are consistent with modest levels of star formation. Similarly, Goto (2004) performed VLA 20 cm radio-continuum observations of 36 E+A galaxies drawn from the SDSS and found that none of these galaxies were detected in the radio wavelengths. These results are supported by Galaz (2000) who do not find compelling evidence for strong internal dust extinction in their E+A sample.

Some E+A galaxies exhibit morphological disturbances indicative of interactions with near neighbours. Yang et al. (2004) have studied the morphologies of the five bluest E+A galaxies in the sample of Zabludoff et al. (1996) using the WFPC2 camera on board the *Hubble Space Telescope* (*HST*) and found that four out of these five galaxies display morphological disturbances consistent with recent mergers. Similarly, Goto (2004) have shown, using the largest sample of E+A galaxies studied to date, that these systems have an excess of local galaxy density at spatial scales less than 100 kpc but not at scales spanned by galaxy clusters (~ 1 Mpc) or large-scale structure (~ 8 Mpc). They find that ~ 30 percent of E+A galaxies exhibit morphological disturbances, indicating that their evolution is linked, at least partially, to mergers and interactions. It is worth noting that, although the Goto (2004) sample is larger and their results are statistically more robust, detection of small, low-surface brightness

(tidal) features probably requires both deeper and higher resolution imaging than that provided by the SDSS. Hence, the fraction of E+A galaxies with tidal tails may well be higher than ~ 30 percent in the Goto (2004) sample, making the conclusions from these two studies more consistent.

From a theoretical perspective, the merger hypothesis is supported by numerical simulations which indicate that gas-rich mergers are capable of triggering strong star formation episodes. The immediate aftermath of such an event is predicted to be a largely spheroidal remnant with a blue core, widespread morphological disturbances such as tidal tails and young star clusters (e.g. Mihos & Hernquist 1994; Bekki et al. 2001). Indeed, the study of Yang et al. (2004) has found a striking correspondence between the predicted properties of merger remnants and the observed characteristics of blue E+A galaxies.

Numerous authors have studied E+A galaxies using a variety of indicators, which allows us to infer the characteristics of the (recent) starburst that dominates the spectra of these systems. While the age of the burst should be approximately ~ 1 Gyr, simply by virtue of A-type stars being present, the mass fractions forming in the burst are inferred to be quite high. Yang et al. (2004) estimate that 50 percent of the mass may form in the burst, allowing the E+A galaxies to fade on to the E/S0 fundamental plane in a few Gyrs after the event. Norton et al. (2001), who analysed the entire Zabludoff et al. (1996) sample, estimate that the fraction of stellar mass in young (A-type) stars is typically between 30 and 80 percent. Bressan et al. (2001) infer a similarly high mass fraction of 60 percent for the sample of E+A galaxies in Poggianti et al. (2001), while Liu & Green (1996) derive mass fractions typically greater than 20 percent (and as high as 100 percent) for eight E+A galaxies taken from the literature (but note that Liu et al. (2007) revise the inferred mass fraction to lower values for one of their E+A galaxies - G515). While E+A's are, by definition, presently quiescent, an estimate of the star formation rate (SFR) that *might* have characterised the recent starburst can be estimated from dusty starburst galaxies which show an E+A signature in their spectra. Poggianti & Wu (2000) estimate the SFRs in these systems to be between 50 and 300 M_{\odot} per year.

While mergers and interactions might trigger star formation, the exact mechanism by which the starburst is subsequently quenched remains largely unexplained. Star formation is, of course, inherently subject to 'negative feedback', since the star formation rate (SFR) depends on the mass of cold gas available. As star formation proceeds and the gas reservoir is exhausted, the rate of further star formation activity correspondingly decreases. However, the properties of E+A galaxies are generally inconsistent with such a gradual, self-modulated decline in the SFR and imply a more abrupt quenching of star formation activity.

Common sources of kinetic and thermal 'feedback' that might be capable of quenching star formation, e.g. by ejecting or heating the gas reservoir, include supernovae (SN), which are effective mainly in low-mass galaxies due to their shallow potential wells, and AGN, which are thought to operate in massive galaxies where SN feedback is not energetic enough to 'disable' the cold gas reservoir. Goto (2006) have demonstrated that some galaxies which contain signatures of an active AGN also exhibit post-starburst signatures, in-

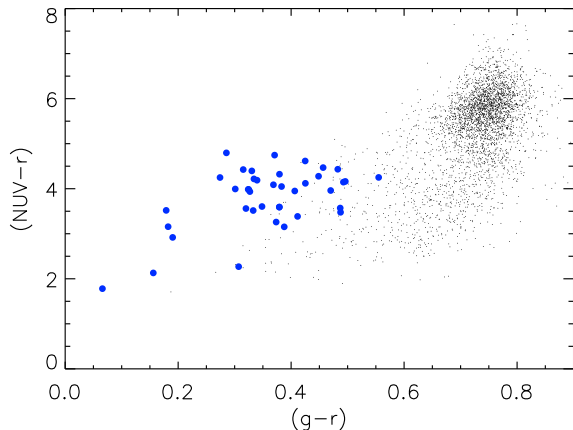


Figure 1. The position of our E+A galaxies (filled blue circles) in the $(NUV - r)$ vs $(g-r)$ colour space, compared to a sample of early-type galaxies drawn from the SDSS DR5 using the method of Kaviraj et al. (2006b) and cross-matched with GALEX. The E+A population inhabits the blue cloud and is well separated from the early-type galaxies which define the bulk of the red sequence. Note that the colours are in the observed frame i.e. they are shown without applying K-corrections.

indicating that a connection exists between these two phenomena. They find that the post-starburst regions are centred around the AGN, the spatial proximity implying that AGN activity could plausibly affect the region around it. Indeed, the fact that the AGN *outlives* the starburst is an indication that it may have played a role in the quenching of star formation.

In this study we extend the existing literature on post-starburst galaxies by performing the first study of E+A systems that incorporates their ultraviolet (*UV*) photometry. The extreme sensitivity of the *UV* to young stars allows us to put strong constraints on the star formation history (SFH) of galaxies within the last ~ 2 Gyrs. The addition of *UV* photometry alleviates the age-metallicity degeneracy that commonly plagues optical studies (Kaviraj et al. 2007), allowing us to better quantify the recent SFH than can be achieved using optical data alone. Indeed, the sensitivity of the *UV* to young stars has recently been exploited to demonstrate that early-type galaxies, traditionally thought to be entirely quiescent systems, exhibit *widespread* evidence for low-level recent star formation, consistent with the expectations of the standard LCDM model (Kaviraj et al. 2006a).

In this paper, we exploit the properties of the *UV* to accurately reconstruct the recent star formation history of individual E+A galaxies. By comparison to a large library of models we derive estimates for the ages of the recent bursts, the mass fractions formed in them and the timescales over which they occurred. By comparing the derived timescales to the dynamical timescales of the galaxies, we explore the efficiency with which star formation has been quenched in these systems and study how this quenching efficiency varies as a function of galaxy properties such as mass, luminosity and stellar velocity dispersion. We use simple energetic arguments to study whether the characteristics of the quenching are consistent with feedback from supernovae and AGN. Fi-

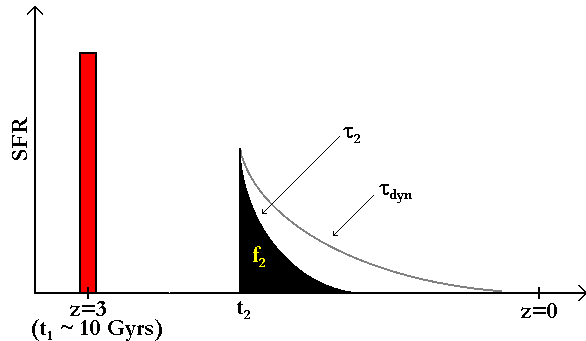


Figure 2. Model SFHs (see Section 2) are constructed by assuming that an instantaneous burst of star formation at high redshift ($z \sim 3$) is followed by a second burst, modelled as an exponential. The free parameters are the age (t_2), mass fraction (f_2) and timescale (τ_2) of the second burst. t_2 is allowed to vary from 0.05 Gyrs to the look-back time corresponding to $z = 3$ in the rest-frame of each E+A galaxy. f_2 varies between 0 and 1 and τ_2 is allowed to vary from 0.01 Gyrs to 4 Gyrs. τ_{dyn} indicates the dynamical timescale of the galaxy. More catastrophic quenching leads to smaller values of the ratio τ_2/τ_{dyn} , which is used in Section 5 to parametrise the *efficiency* with which quenching occurs in the E+A galaxies studied here.

nally, we study the timescale over which E+A galaxies can evolve from their present positions in the blue cloud to the red sequence. Since E+As are, by definition, at the point of truncation of their star formation, it is possible to get a rather ‘clean’ estimate of this migration timescale by studying the evolution in both *UV* and optical colours.

2 SAMPLE SELECTION

We use the publicly available Garching SDSS catalog¹ to select E+A galaxies from the SDSS DR4. The criteria used for E+A selection follow that of Goto (2005): $H\delta$ (EW) $> 5.0\text{\AA}$ (measured in the wider window of 4082-4122 \AA), $H\alpha$ (EW) $> -3.0\text{\AA}$, [OII] (EW) $> -2.5\text{\AA}$. Absorption lines have a positive sign in these definitions. Note that including the equivalent width of the $H\alpha$ line makes the selection criteria stronger, because using *only* the [OII] line could result in more than 50 percent of the selected galaxies having measurable $H\alpha$ emission (e.g. Goto et al. 2003). In addition to the line measurements we also use estimates of stellar mass and AGN classifications provided by the Garching SDSS catalog. The line index measurements in this catalog were calculated using the code of Tremonti et al. (2004), while stellar mass estimates and AGN classifications were taken from a series of comprehensive analyses of the local galaxy population observed by the SDSS (Kauffmann et al. 2003a; Kauffmann et al. 2003b; Brinchmann et al. 2004)

To ensure the accuracy of the line measurements, the sample was restricted to galaxies where the median S/N of the spectrum is greater than 10. Galaxies which show evidence of an active AGN were removed, because scattered light from the AGN could contaminate the *UV* continuum and affect the derived parameters presented later in this

¹ <http://www.mpa-garching.mpg.de/SDSS/DR4/>

analysis. Finally, the sample was restricted to galaxies in the redshift range $0 < z < 0.2$, since the *UV* filters used in the analysis (see below) trace flux blueward of the *UV* continuum at higher redshifts.

This E+A sample, drawn from the SDSS DR4, was then cross-matched with publicly available *UV* photometry from the second data release of the GALEX mission (Martin et al. 2005). GALEX provides two *UV* filters: the far-ultraviolet (*FUV*), centred at $\sim 1530\text{\AA}$ and the near-ultraviolet (*NUV*), centred at $\sim 2310\text{\AA}$. This cross-matching produced 38 E+A galaxies which have *at least* a detection in the *NUV* filter, 28 of which have photometry in both the *FUV* and *NUV* filters.

Figure 1 shows the position of our E+A galaxies (filled blue circles) in the $(NUV - r)$ vs $(g - r)$ colour space, compared to a sample of early-type galaxies drawn from the SDSS DR5 using the method of Kaviraj et al. (2006b) and cross-matched with the GALEX second data release. It is apparent that the E+A population is well separated from the early-type population which defines the bulk of the red sequence. Comparison to Figure 1 in Yi et al. (2005) indicates that E+A galaxies inhabit the blue cloud.

Since previous studies have indicated that E+A galaxies are potential progenitors of early-type galaxies, we check the morphologies of the E+A galaxies in our sample using the SDSS *fracDev* parameter. The SDSS pipeline fits both deVaucouleur’s and exponential surface brightness profiles to galaxy images (in each filter) and creates a composite *best-fit* profile using a linear combination of the two fits. The *fracDev* parameter is the weight of the deVaucouleur’s profile in this composite fit. Thus, galaxies with large values of *fracDev* can be considered to have spheroidal morphology. We find that all but 6 of the galaxies studied in this sample have *fracDev* > 0.8 in the *r*-band, which indicates that the majority of E+A galaxies in this sample are indeed spheroidal systems. It is worth noting that all 6 galaxies which have *fracDev* < 0.8 are low-mass systems ($M < 10^{10}M_{\odot}$) and their non-deVaucouleur’s morphologies are consistent with the fact that dwarf ellipticals typically show exponential surface brightness profiles.

3 PARAMETER ESTIMATION

We estimate parameters governing the star formation history (SFH) of each E+A galaxy by comparing their (*FUV*, *NUV*, *u*, *g*, *r*, *i*, *z*) photometry to a library of synthetic photometry generated using a large collection of model SFHs. Each SFH is constructed by assuming that an instantaneous burst of star formation at high redshift ($z \sim 3$) is followed by a second burst which is modelled as an exponential.

Figure 2 shows a schematic representation of the model SFHs. The free parameters in this analysis are the age (t_2), mass fraction (f_2) and timescale (τ_2) of the second burst. t_2 is allowed to vary from 0.05 Gyrs to the look-back time corresponding to $z = 3$ in the rest-frame of each E+A galaxy. f_2 varies between 0 and 1 and τ_2 is allowed to vary from 0.01 Gyrs to 4 Gyrs. Since our focus is purely on E+A galaxies, we must, by definition, exclude models which contain ongoing star formation. Therefore, we only keep models where the intensity of star formation in the second burst

at present-day is less than 5 percent of the intensity when the burst started². Changing this threshold to less than 5 percent leaves our results unchanged. Note that excluding models that have ongoing star formation reduces the allowed parameter space of model SFHs, resulting in much tighter constraints on the parameters, in particular, the timescale of star formation τ_2 .

The motivation for an instantaneous burst at high redshift stems from the fact that, as potential progenitors of spheroidal galaxies, one expects a substantial fraction of stellar mass to have formed at high redshift in these galaxies (e.g. Bower et al. 1992, Kaviraj et al. 2006b). Furthermore, since the *UV* is insensitive to stellar populations older than ~ 2 Gyrs coupled with the fact that optical colour evolution virtually stops after 5-6 Gyrs (e.g. Yi 2003), resolving this old burst does not affect the *UV* and optical colours of the model.

The *UV* flux in each model is completely dominated by the second burst of star formation. Even though our expectations, on the basis of the properties of E+A galaxies (and previous studies of E+A systems), are that $t_2 \sim 1$ Gyr and f_2 is high, our model library does not put a prior on these parameters - vigorous starbursts at recent epochs are allowed, as is slowly declining star formation from intermediate redshifts. In essence, the comparison between the synthetic library and observed photometry is allowed to ‘choose’ the optimum SFH that satisfies the photometry of each E+A galaxy.

To build the library of synthetic photometry, each model SFH is combined with a single metallicity in the range $0.1Z_{\odot}$ to $2.5Z_{\odot}$ and a value of dust extinction parametrised by $E(B-V)$ in the range 0 to 0.5. Photometric predictions are generated by combining each model SFH with the chosen metallicity and $E(B-V)$ values and convolving with the stellar models of Yi (2003) through the GALEX *FUV*, *NUV* and SDSS *u*, *g*, *r*, *i*, *z* filters. This procedure yields a synthetic library of 1.5 million models.

Since our E+A galaxies are observed at a range of redshifts, equivalent libraries are constructed at redshift intervals of $\delta z = 0.01$. A fine redshift grid is essential in such a low redshift study because a small change in redshift produces a relatively large change in look-back time over which the *UV* flux can change substantially, inducing ‘K-correction-like’ errors into the analysis.

The free parameters (t_2 , f_2 and τ_2) are estimated by comparing each observed galaxy to every model in the synthetic library, with the likelihood of each model ($\exp -\chi^2/2$) calculated using the value of χ^2 computed in the standard way. From the joint probability distribution, each parameter is marginalised to extract its one-dimensional probability density function (PDF). We take the median of this PDF as the best estimate of the parameter in question and the 16 and 84 percentile values as the ‘one-sigma’ uncertainties on this estimate. The cosmological parameters used in this study assume a Λ CDM model: $h = 0.7$, $\Omega_m = 0.3$ and $\Omega_{\Lambda} = 0.7$.

Note that there are 10 galaxies in our sample which do not have *FUV* detections. The parameter estimation on

² This implies that models with small values of t_2/τ_2 are excluded.

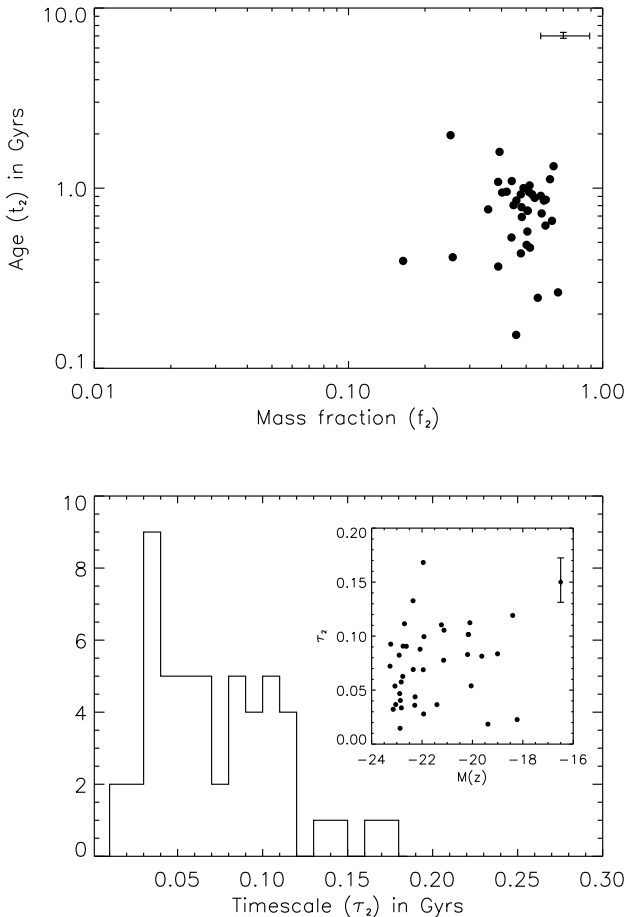


Figure 3. TOP PANEL: Ages and mass fractions of the burst that creates the E+A galaxies in our sample. Burst ages are typically within a Gyr, as one expects from the lifetimes of A-type stars which contribute significantly to E+A spectra. We recover large mass fractions, typically higher than 10 percent and possibly as high as 70 percent, consistent with previous studies. BOTTOM PANEL: Effective timescales of the starbursts in E+A galaxies. The timescales are typically short - between 0.01 and 0.2 Gyrs - implying that the star formation rates during the burst phase are high (see text in Section 4 and Figure 4).

these galaxies is carried out using only the *NUV*, *u*, *g*, *r*, *i* and *z*-band filters. We do not use the *FUV* detection limit as an upper limit to the *FUV* flux.

4 CHARACTERISTICS OF THE RECENT BURST: AGES, MASS FRACTIONS AND TIMESCALES

We begin by presenting estimates for the basic parameters (t_2 , f_2 and τ_2) that describe the burst of star formation that immediately precedes the quenching in our E+A galaxies. The top panel of Figure 3 shows the ages and mass fractions of the recent burst in each E+A galaxy. The burst ages are typically within 2 Gyrs, as one expects from the lifetimes of A-type stars which contribute significantly to E+A spectra. In agreement with previous studies, we derive large mass

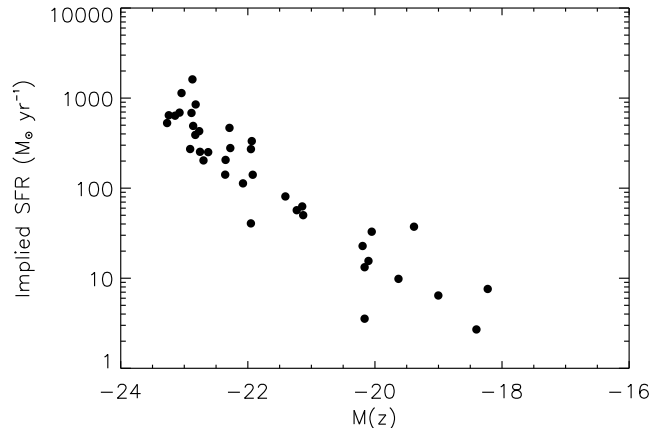


Figure 4. Implied SFRs during the burst phase in E+A galaxies. The implied SFR is estimated by dividing the stellar mass formed by the timescale of the burst. Note that, since the burst lasts longer than one timescale, the SFRs are overestimated. However, the estimates probably give a reasonable indication of the SFR during the most intense period of the starburst.

fractions, which are typically higher than 10 percent and possibly as high as 70 percent in some galaxies. The bottom panel shows the timescales over which the bursts take place. The timescales are typically short - between 0.01 and 0.2 Gyrs - implying that the star formation rates during the burst phase are extremely high.

We can estimate this ‘implied’ SFR by dividing the stellar mass formed by the timescale of the burst (Figure 4). We note that, since the burst lasts longer than one timescale, the SFRs are overestimated. However, the estimates probably give a reasonable indication of the SFR during the most intense period of the starburst and we find a tight correlation between the mass of the E+A galaxy and the implied SFR. (see bottom panel of Figure 3). While low-luminosity ($M(z) > -20$) E+As have implied SFRs of less than $50 M_{\odot} yr^{-1}$, E+A systems at the high-luminosity end ($M(z) < -22$) exhibit SFRs of greater than 300, and as high as $2000 M_{\odot} yr^{-1}$.

The high SFRs inevitably lead to comparisons with luminous and ultra-luminous infrared galaxies (LIRGs/ULIRGs), whose high infrared luminosities ($L_{IR} > 10^{11} L_{\odot}$) imply massive ongoing starbursts (e.g Sanders & Mirabel 1996). SFRs in LIRGs ($10^{11} L_{\odot} < L_{IR} < 10^{12} L_{\odot}$) typically exceed a few tens of solar masses per year, while in ULIRGs ($L_{IR} > 10^{12} L_{\odot}$) the SFRs can be as high as hundreds of solar masses per year (e.g. Kennicutt 1998). Wang et al. (2006), who have performed a study of LIRGs in the nearby Universe ($z \sim 0.1$), find SFRs of between 10 and $100 M_{\odot} yr^{-1}$ for their sample of galaxies (see their Figure 5). Noting that our SFRs are overestimated, and could be a few factors too high, we suggest that LIRGs at low redshift *could* transform into massive E+A galaxies. However, we note that the robustness of such a conclusion depends on performing an identical parameter estimation on LIRGs at low redshift and by considering whether other factors, such as the local environments of E+A galaxies, correspond closely to those of LIRGs.

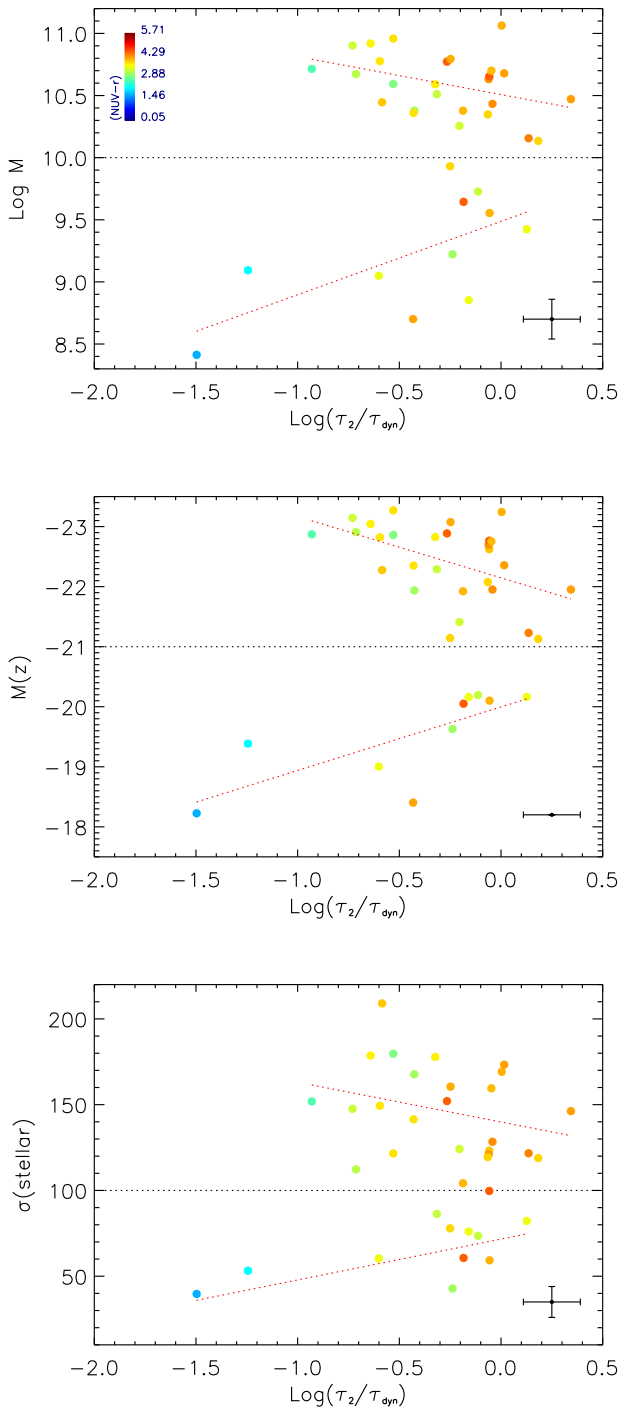


Figure 5. The timescale ratio, $r_\tau = \tau_2/\tau_{dyn}$, plotted against galaxy mass (top), absolute z-band luminosity (middle) and stellar velocity dispersion (bottom). Note that the red dotted lines indicate standard least-squares fits to the data. The fits are performed separately for the massive ($M > 10^{10} M_\odot$) and low-mass ($M < 10^{10} M_\odot$) E+A galaxies in each panel.

5 THE EFFICIENCY OF QUENCHING AS A FUNCTION OF GALAXY MASS

One of the primary goals of this paper is to study the characteristics of the quenching that truncates the burst and determine the possible mechanisms by which this quenching could occur. A key parameter in this analysis is the *efficiency* with which the star formation is quenched. We study this ‘quenching efficiency’ by comparing the effective timescale of the burst, τ_2 , to the dynamical timescale³ of the galaxy, τ_{dyn} , which is defined as

$$\tau_{dyn} = \left(\frac{2R^3}{GM} \right)^{1/2}, \quad (1)$$

and describes the ‘natural’ timescale over which processes such as star formation would take place if left *unhindered*⁴. Note that, in the calculations that follow, we have used the stellar mass of the galaxy as the value of M . We parametrise the quenching efficiency by constructing the timescale ratio

$$r_\tau = \tau_2/\tau_{dyn}. \quad (2)$$

More efficient quenching reduces τ_2 and therefore produces a lower value for r_τ . The timescale ratio is, therefore, *inversely correlated* with quenching efficiency - more catastrophic quenching results in lower values of r_τ .

In Figure 5 we plot r_τ against three independent indicators of galaxy mass/luminosity. The galaxies are colour-coded using their $(NUV-r)$ colour. The plot of r_τ vs galaxy mass (top panel), reveals a striking difference in the behaviour of r_τ with increasing galaxy mass. We find that, below a mass of $10^{10} M_\odot$, the quenching efficiency decreases with increasing galaxy mass. However, when the galaxy mass is greater than $\sim 10^{10} M_\odot$ this trend is reversed and the quenching efficiency then correlates positively with the galaxy mass. We check this behaviour with both $M(z)$ and stellar velocity dispersion. We find that the correlation of r_τ with galaxy mass and, in particular, its apparent reversal is present in all the separate indicators of galaxy mass/luminosity. While a strong trend is apparent with stellar mass (M) and z band luminosity, the trend is weaker in the stellar velocity dispersion (σ), most probably driven by bigger uncertainties in the σ measurement (as suggested by the larger scatter in this plot). A plausible source of uncertainty is the fact that the E+A galaxies are unrelated (indeed a significant fraction look disturbed in the SDSS images), implying that σ does not yet trace the virial mass of the galaxy. An additional source of uncertainty is the presence of a substantial young stellar population. The presence of young sub-components could create a bias towards lower values of σ , with the magnitude of the bias driven by the mass fraction and age of the young stars and on the exact size of the physical aperture subtended by the SDSS spectra in each galaxy. We therefore suggest that the correlation be-

³ Using $s = \frac{1}{2}at^2$ from the equations of motion, the dynamical timescale follows by setting $a = g = (GM/R^2)$ and $s = R$.

⁴ Note that we use the radius that contains 90 percent of the Petrosian flux in the i -band as the value of R .

tween r_τ and σ should be treated with caution considering the caveats we have presented above.

Figure 5 shows that the reversal in the r_τ correlation occurs at $M \sim 10^{10} M_\odot$, $M(z) \sim -21$ and $\sigma \sim 100 \text{ kms}^{-1}$ when r_τ is plotted against mass, absolute z-band luminosity and stellar velocity dispersion respectively. The dichotomy in the trend of r_τ against galaxy mass indicates that the principal quenching mechanisms for galaxies above and below the mass threshold of $10^{10} M_\odot$ behave very differently. In particular, the mechanism that operates in the regime $M < 10^{10} M_\odot$ becomes *weaker* as the galaxy mass increases while the mechanism that operates in the regime $M > 10^{10} M_\odot$ becomes *stronger* as the galaxy mass increases.

The mass threshold ($10^{10} M_\odot$) at which the r_τ vs. M trend reverses is particularly interesting because it is in excellent agreement with the mass above which AGN become significantly more abundant in galaxies in the nearby Universe (Kauffmann et al. 2003a). Given this result, the reversal at $M \sim 10^{10} M_\odot$ can be explained, at least qualitatively, in terms of SN and AGN being the principal quenching sources above and below this mass threshold. In the absence of AGN, the primary source of negative feedback are SN. As galaxies become more massive and the depth of the potential well increases, SN find it increasingly more difficult to eject gas from the system. This results in the quenching becoming less efficient at higher galaxy masses, exactly as we observe in Figure 5.

However, once AGN begin to appear (above $M \sim 10^{10} M_\odot$), they become the dominant source of negative feedback. For a $10^{11} M_\odot$ galaxy, the energy input from a population of (Type II) SN formed as a result of a starburst that creates half the stellar mass of the galaxy is $\sim 3 \times 10^{57} \text{ ergs}^5$, while the energy output from a central AGN, emitting at the Eddington limit⁶ over a timescale of 0.1 Gyrs is $\sim 3 \times 10^{58} \text{ ergs}^7$. In terms of energy input the AGN dominates and it is reasonable to assume that it dictates the mechanics of the quenching. Note that we did not consider Type Ia supernovae in this calculation because the derived timescales (see Figure 3) are considerably shorter than 1 Gyr, which is the typical time delay between the onset of star formation and the appearance of Type Ia supernovae.

Given that the mass of the black hole (M_{BH}) scales with the central velocity dispersion σ as $M_{BH} \sim \sigma^\beta$ (Gebhardt et al. 2000; Ferrarese & Merritt 2000), where β

⁵ The energy injected by a population of SN is given by $\eta_{SN} \varepsilon_{SN} \Delta M$, where $\eta_{SN} (\sim 5 \times 10^{-3} M_\odot^{-1})$ is the number of SN per unit stellar mass and $\varepsilon_{SN} (\sim 10^{51} \text{ ergs})$ is the energy supplied by each supernova. The fraction of that energy that couples mechanically to the material in the ISM is approximately given by $\sigma/20,000 \text{ kms}^{-1}$, where σ is the velocity dispersion and $20,000 \text{ kms}^{-1}$ is the velocity of the SN ejecta. For a $M \sim 10^{11} M_\odot$ galaxy, $\sigma \sim 200 \text{ kms}^{-1}$.

⁶ The Eddington luminosity for a mass M is $\sim 1.3 \times 10^{38} M/M_\odot$ ergs per second.

⁷ A $M \sim 10^{11} M_\odot$ typically hosts a $M \sim 10^8 M_\odot$ black hole, since $(M_{BH}/M_{bulge}) \sim 10^{-3}$ (Haring & Rix 2004). The Eddington luminosity of such a black hole is $\sim 10^{46} \text{ ergs s}^{-1}$, of which a fraction $\sigma/c \text{ kms}^{-1}$ couples to the mechanically to the material in the ISM. σ is the velocity dispersion of the galaxy and c is the speed of light.

varies in range 4-5, and assuming the energy outputted by the AGN scales with M_{BH} (c.f. the Eddington luminosity $L_{edd} \propto M_{BH}$), we expect AGN feedback to become more effective, and thus the quenching efficiency to increase, as galaxy mass increases. Again, this is indeed what we observe in Figure 5. We briefly note that, by definition, our sample does not contain galaxies that show signs of *current* AGN activity, implying that the AGN has shut itself off in the process of providing feedback. If, as we argue below, mechanical feedback from the AGN depletes the gas reservoir, then this process also removes the AGN’s own fuel source. Thus it is plausible that the feedback process *simultaneously* quenches both star formation and AGN activity.

It is worth noting that a similar dichotomy in the primary feedback mechanism has been inferred by (Shankar et al. 2006), from a study of the stellar and baryonic mass functions of galaxies, extracted using the mass-to-light ratios of stars and gas derived from galaxy kinematics.

6 THE EXPECTED DEPENDENCE OF THE QUENCHING EFFICIENCY ON GALAXY MASS

We now use simple energetic arguments to derive the expected relationship between the timescale ratio r_τ and galaxy mass in the two cases where the quenching is due to SN and AGN respectively.

We make the assumption that quenching takes place due to the ejection of available gas from the potential well. The energy required for quenching, E_q , is given by,

$$E_q = \frac{1}{2} m_g v_{esc}^2, \quad (3)$$

where m_g is the mass of gas to be ejected and v_{esc}^2 is the escape velocity. Since,

$$v_{esc}^2 = \left(\frac{2GM}{R} \right), \quad (4)$$

this implies that

$$E_q \propto m_g \cdot \frac{M}{R}, \quad (5)$$

or equivalently, in terms of parameters derived in this analysis that,

$$E_q \propto m_g \cdot \left(\frac{M}{\tau_{dyn}} \right)^{2/3} \propto m_g \cdot \left(\frac{M r_\tau}{\tau_2} \right)^{2/3}. \quad (6)$$

The relationships in Eqn (6) use substitutions from Eqns (1) and (2). Eqn (6) describes the dependence of the energy required for quenching on the timescale ratio r_τ , the burst timescale τ_2 and galaxy mass M .

We now make the simplifying assumption that the mass of gas (m_g) required to be ejected for quenching is approximately constant in all galaxies. This is consistent with the downsizing phenomenon (e.g Cowie et al. 1996), whereby smaller galaxies exhibit higher star formation rates than their massive counterparts at lower redshifts. Given the apparent universality of the Schmidt-Kennicutt law for (quiescent) star formation (Kennicutt 1998), downsizing implies

that smaller galaxies tend to be more gas-rich than larger ones, justifying the empirical assumption that their *absolute* neutral gas reservoirs may have similar sizes. Cold gas fractions in low-redshift LIRGs (see Figure 5 in Wang et al. 2006), which are potential progenitors of E+A galaxies (Section 4), indeed show a declining trend with galaxy mass. Across the mass range $10^{10.5} - 10^{11.5} M_{\odot}$, the gas fractions increase from less than 5 percent to greater than 25 percent, suggesting that the cold gas reservoirs in these galaxies are similar in size and that our assumption of constant m_g is a reasonable one. A small spread in the real values of m_g will induce a scatter in the trends derived in Section 6.1 and 6.2 below, without perturbing the correlations between the variables. With this assumption Eqn (6) becomes

$$E_q \propto \left(\frac{M}{\tau_{dyn}}\right)^{2/3} \propto \left(\frac{M r_{\tau}}{\tau_2}\right)^{2/3}. \quad (7)$$

We should also note that the assumption that quenching occurs through the mechanical ejection of gas may imply that E+A galaxies should be relatively gas-poor, although the gas could simply be dispersed away from the central regions of the potential well where star formation would normally take place. Two studies of the *HI* content of E+A galaxies have been conducted so far. Chang et al. (2001) observed five E+A galaxies from the Zabludoff et al. (1996) sample and detected only one with an *HI* mass of $\sim 3.4 \times 10^9 M_{\odot}$. Similarly, Buyle et al. (2006) detected similar amounts ($> 10^9 M_{\odot}$) of *HI* in three out of six E+A galaxies they observed in *HI*. While, it might be useful to compare the gas masses estimated by Buyle et al. (e.g 2006) for E+A galaxies to those estimated for LIRGs (as potential progenitors) by Wang et al. (2006), the mass ranges traced by these two studies are quite different. Buyle et al. (2006) trace galaxies with $M \lesssim 10^{10.7} M_{\odot}$ ⁸, while Wang et al. (2006) study galaxies with $M \gtrsim 10^{10.6} M_{\odot}$. The small overlap region around $10^{10.7} M_{\odot}$ indicates that the *HI* fraction⁹ in the LIRGs may be higher by a factor of 3. We note, however, that due to the inadequate overlap between the two samples, this result is not very robust. However, given the apparent lack of *HI* in the majority of E+A's observed by Chang et al. (2001) and the smaller gas fractions found in Buyle et al. (2006) compared to nearby LIRGs (which have comparable SFRs to our E+A galaxies) the assumption of quenching through the mechanical ejection of gas seems reasonable.

6.1 Quenching by supernovae

The energy injected by SN into the ISM is proportional to the amount of stellar mass produced in the burst so that

⁸ The masses of the Buyle et al. (2006) galaxies have been estimated by converting the values of $M(B)$ given in their Table 1 to $M(z)$, which are then converted to masses using the M vs. $M(z)$ relation for the E+A galaxies in our sample.

⁹ Note that we have converted the H_2 mass (which is the quantity estimated by Wang et al. (2006)) to an *HI* mass, using the average *HI*/ H_2 ratio for late-type galaxies (~ 0.6) given by Fukugita et al. (1998, see their Table 1)

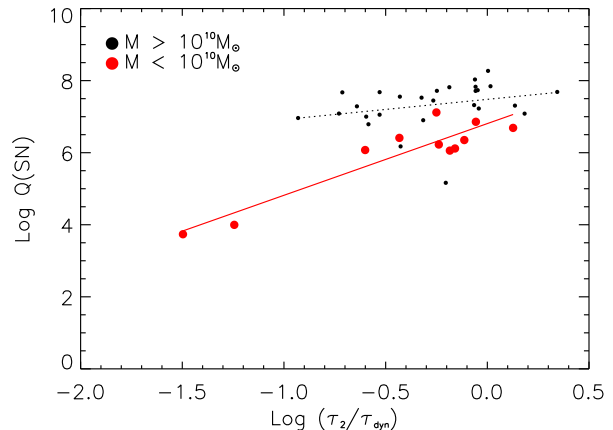


Figure 6. r_{τ} vs. Q_{SN} for galaxies with $M > 10^{10} M_{\odot}$ (black) and $M < 10^{10} M_{\odot}$ (red). The solid lines indicate standard least-squares fits to the data.

$$E^{SN} = \eta_{SN} \varepsilon_{SN} \Delta M, \quad (8)$$

where η_{SN} is the number of SN per unit stellar mass, ε_{SN} is the energy supplied by each supernova and ΔM is the amount of stellar mass formed. Hence,

$$E^{SN} \propto f_2 M, \quad (9)$$

since $\Delta M = f_2 M$. Combining Eqn (7) and Eqn (9) gives,

$$r_{\tau}^2 \propto \tau_2^2 f_2^3 M, \quad (10)$$

so that

$$\log(\tau_2^2 f_2^3 M) = 2 \log(r_{\tau}) + k \quad (11)$$

As we would naively expect from SN driven feedback, r_{τ} correlates with the galaxy mass (M). Since r_{τ} is inversely correlated to the quenching efficiency, this implies that, as galaxy mass increases, the quenching efficiency decreases in the SN feedback scenario. Defining $Q_{SN} = \tau_2^2 f_2^3 M$ we have,

$$\log(Q_{SN}) = 2 \log(r_{\tau}) + k, \quad (12)$$

where k absorbs the constants in the proportionality relations used to derive Eqn (12). A plot of $\log(Q_{SN})$ against $\log(r_{\tau})$ should therefore show a gradient of 2, if the systems being considered are indeed quenched *purely* by SN.

In Figure 6 we plot r_{τ} vs. Q_{SN} for both low-mass ($M < 10^{10} M_{\odot}$; black) and massive ($M > 10^{10} M_{\odot}$; red) galaxies. The solid lines indicate standard least-squares fits to the data. We find that, while low-mass galaxies show a gradient of 1.98 ± 0.18 (and are therefore consistent with the expected gradient of 2), the best-fit relation for the massive galaxies is too shallow (0.56 ± 0.06) and does not satisfy the predictions. We conclude, therefore, that low-mass galaxies show good consistency with being quenched *purely* by SN

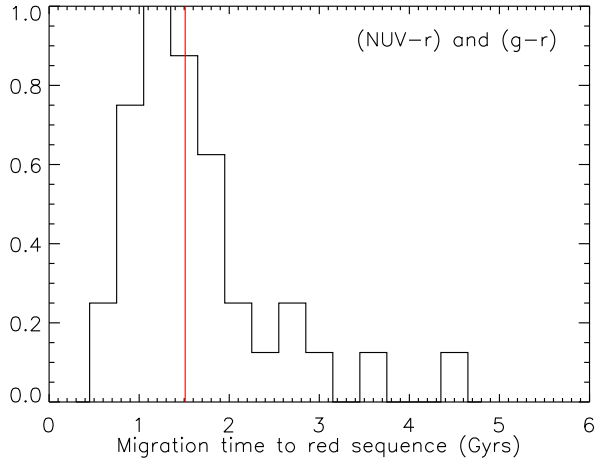


Figure 7. Histogram showing the migration time of E+A galaxies from the blue cloud to the red sequence in both the *UV* and optical colours. The median migration time (indicated by the solid red line is ~ 1.5 Gyrs. The y-axis shows the frequency normalised to 1.)

feedback while massive galaxies are essentially inconsistent with such a picture.

6.2 Quenching by AGN

The energy injected by an AGN (E^{AGN}) is driven by its luminosity (L) so that,

$$E^{AGN} \propto L \cdot \tau_2. \quad (13)$$

Rewriting Eqn (13) in terms of the Eddington luminosity (L_{edd}), we have

$$E^{AGN} \propto \mu \cdot L_{edd} \cdot \tau_2, \quad (14)$$

where $\mu = L/L_{edd}$ is the Eddington ratio. L_{edd} is proportional to the mass of the central black hole (M_{BH}), which in turn has been shown to scale with the central velocity dispersion (σ) of the galaxy as $M_{BH} = \sigma^\beta$. Estimates of β vary in the range 4-5, with Gebhardt et al. (e.g. 2000) reporting $\beta = 3.75 \pm 0.3$, while Ferrarese & Merritt (2000) report $\beta = 4.8 \pm 0.5$. For simplicity, we begin by assuming that μ is constant across our entire sample of AGN. Then,

$$E^{AGN} \propto \sigma^\beta \cdot \tau_2. \quad (15)$$

Since, the virial theorem¹⁰ implies that $\sigma^2 \sim M/R$ we rewrite this as,

$$E^{AGN} \propto \frac{M^{\beta/3} r_\tau^{\beta/3}}{\tau_2^{\beta/3}} \cdot \tau_2, \quad (16)$$

¹⁰ The virial theorem states that, for a system with kinetic energy K and potential energy U , $2K + U = 0$. For a mass distribution of mass M and radius R , $K \sim \frac{1}{2} M \sigma^2$ and $U \sim \frac{GM}{R^2}$ which implies that $\sigma^2 \sim M/R$.

where we have used Eqns (1) and (2) to eliminate R and explicitly introduce the timescale ratio r_τ . Equating Eqn (7) and Eqn (16) then gives

$$r_\tau^{(2-\beta)} \propto M^{(\beta-2)} \cdot \tau_2^{(5-\beta)} \quad (17)$$

Using $\beta \sim 5$ from Ferrarese & Merritt (2000) then implies that

$$M \propto r_\tau^{-1} \quad (18)$$

or that

$$\log M = -\log(r_\tau) + k, \quad (19)$$

where k absorbs the constants in the proportionality relations used to derive Eqn (18). We find that a plot of $\log M$ against $\log r_\tau$ should show a gradient of -1, if the systems being considered are indeed quenched by AGN which have similar Eddington ratios, regardless of their size. Eqn (18) explicitly predicts that, for galaxies which are quenched by AGN alone, the quenching efficiency (which is inversely correlated to r_τ) increases as the mass of the galaxy increases.

We now refer back to Figure 5 (top panel), where we have plotted the dependence of r_τ on galaxy mass for both massive and low-mass galaxies. It is clear that low-mass galaxies are inconsistent with the energetics of AGN-driven quenching, since for these systems r_τ correlates positively with galaxy mass. Massive galaxies, on the other hand, do show an inverse correlation with r_τ . However, the observed gradient in the correlation in Figure 5 is -0.36 ± 0.11 , shallower than the predicted gradient of -1.

This discrepancy arises due to our assumption, in Eqn (13), that the Eddington ratio during the burst phase (μ) does not change as a function of host galaxy mass. Clearly, if μ decreases, then the rate of energy output (L) also decreases and a longer timescale (τ_2) is required to inject the same amount of energy. This, in turn, implies a larger value of r_τ .

We now refine our previous analysis by allowing the Eddington ratio to vary as a function of mass so that,

$$\mu = M^\gamma \quad (20)$$

With this dependence on M , Eqn (16) becomes

$$E^{AGN} \propto \frac{M^{\beta/3} r_\tau^{\beta/3}}{\tau_2^{\beta/3}} \cdot \tau_2 \cdot M^\gamma, \quad (21)$$

so that,

$$r_\tau^{(2-\beta)} \propto M^{(3\gamma+\beta-2)} \cdot \tau_2^{(5-\beta)}. \quad (22)$$

Using $\beta \sim 5$ as before then gives,

$$M \propto r_\tau^{-1/(1+\gamma)}. \quad (23)$$

Comparison with the observed gradient of -0.36 ± 0.11 implies that $1 < \gamma < 3$. We find, therefore, that the observed gradient in the $\log M$ vs. $\log r_\tau$ correlation can be reproduced if the Eddington ratio of the E+A galaxies is assumed to vary with M . Since the E+A masses are spread

over an order of magnitude, this implies that the Eddington ratios of the smallest AGN (with host galaxy masses $M \sim 10^{10} M_{\odot}$) in this sample of galaxies are *at least* one-tenth of those for their most massive counterparts in this sample (if $\gamma \sim 1$).

Finally, it is instructive to calculate if a variable Eddington ratio (with $1 < \gamma < 3$) might indeed be expected from simple arguments. The luminosity (L) of an AGN is proportional to the mass accretion rate (\dot{M}). Spherical, Bondi-Hoyle accretion (Bondi & Hoyle 1944) implies that \dot{M} is proportional to the square of the mass of the central black-hole (BH) i.e.

$$L \propto \dot{M} \propto M_{BH}^2. \quad (24)$$

Since the Eddington luminosity (L_{edd}) is proportional to M_{BH} we have,

$$\frac{L}{L_{edd}} \propto M_{BH}. \quad (25)$$

The BH mass is typically a constant fraction of the mass of the bulge (e.g. Häring & Rix 2004), with

$$\frac{M_{BH}}{M_{bulge}} \sim 10^{-3}, \quad (26)$$

which implies that,

$$\mu = \frac{L}{L_{edd}} \propto M, \quad (27)$$

where we have assumed that the E+A galaxies in our sample are bulge-dominated. Such a scenario implies that the expected value of γ in the analysis presented above is ~ 1 , which is consistent with the derived range ($1 < \gamma < 3$).

Assuming a more general dependence of \dot{M} on M_{BH} ($\dot{M} \propto M_{BH}^{\lambda}$), would imply that,

$$\frac{L}{L_{edd}} \propto M^{\lambda-1}. \quad (28)$$

$\lambda - 1$ is equal to γ in Eqn (20) and the Eddington ratio increases with host galaxy mass (as is required to satisfy the shallower gradient in the $\log M$ vs. $\log r_{\tau}$ relation) if $\lambda \gtrsim 2$. For Bondi-Hoyle accretion $\lambda \sim 2$.

7 MIGRATION TIME TO THE RED SEQUENCE

Galaxy colours show a pronounced bimodality over a large range in redshift. This dichotomy in the colours, combined with the build-up of the red sequence over time (e.g. Bell et al. 2004), indicates that a central feature of the evolution of the galaxy population is the net migration of galaxies from the blue cloud onto the red sequence. Therefore, in the context of understanding the macroscopic evolution of galaxies, it is useful to have an estimate of the typical time it takes to complete this migration.

Given the very recent truncation of star formation in these systems, E+A galaxies are just about to begin this migration process. Assuming there is negligible star formation

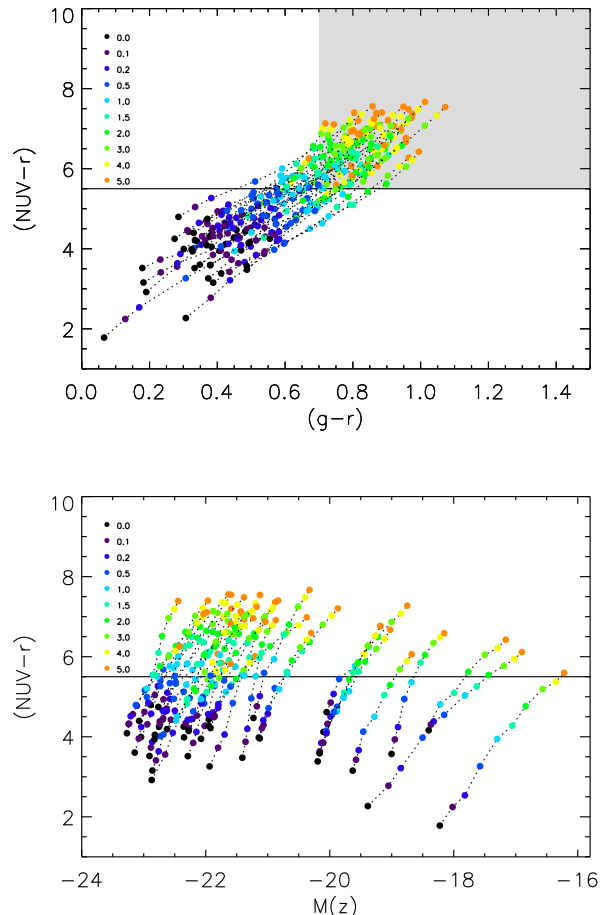


Figure 8. Migration tracks of E+A galaxies in the $(NUV - r)$ vs $(g - r)$ colour space (top panel) and the $(NUV - r)$ vs $M(z)$ colour-magnitude space (bottom panel). Ages (in Gyrs) along the track are shown colour-coded.

during this phase, we can use our derived SFHs to estimate the time it takes for galaxies to move from the blue cloud to the red sequence in *both* the UV and optical colours. The use of E+A galaxies and the fact that we study the migration in *both* the UV and optical spectrum makes the derived migration times quite robust. Note that we define the red sequence as the part of the $(NUV - r)$ vs $(g - r)$ colour space that hosts the bulk of the *red* early-type population. Comparison to Figure 1 indicates that the red sequence lies redward of $(NUV - r) \sim 5.5$ and $(g - r) \sim 0.7$.

We estimate the migration times by ‘ageing’ the *best-fit* model SFHs of each E+A galaxy, keeping secondary parameters such as metallicity and $E(B - V)$ constant. We find that the migration times vary between 1 and 5 Gyrs (Figure 7). Most galaxies complete their migration within 2 Gyrs and the median migration time of galaxies in this sample (shown using the solid red line) is ~ 1.5 Gyrs. Finally, in Figure 8 we show the migration tracks of the E+A sample in the $(NUV - r)$ vs $(g - r)$ colour space (top panel) and the $(NUV - r)$ vs $M(z)$ colour-magnitude space (bottom panel). Ages along the track are shown colour-coded.

8 CONCLUSIONS

We have presented the first study of nearby E+A galaxies which incorporates their *UV* photometry. By exploiting the sensitivity of the *UV* to young stars, we have accurately reconstructed the recent star formation histories of 38 E+A galaxies in the nearby Universe ($0 < z < 0.2$), by combining optical (u, g, r, i, z) and *UV* data from the SDSS and GALEX surveys respectively.

We find that the burst of star formation that dominates the post-starburst signatures in these galaxies typically takes place within a Gyr, which is consistent with the presence of A-type stars in these systems. The stellar mass fractions formed in this burst are typically high, ranging from 20 percent to 60 percent of the mass of the E+A remnant. The timescale over which this star formation takes place is short, ranging between 0.01 and 0.2 Gyrs. The combination of short timescales and high mass fractions imply high SFRs during the burst. We find a tight, positive correlation between the mass of the E+A galaxy and the implied SFR. While low-luminosity ($M(z) > -20$) E+As have implied SFRs of less than $50 M_{\odot} \text{yr}^{-1}$, E+A systems at the high-luminosity end ($M(z) < -22$) exhibit SFRs of greater than 300, and as high as $2000 M_{\odot} \text{yr}^{-1}$. The SFRs are comparable to those found in LIRGs and ULIRGs at low redshift and our results indicate that massive LIRGs at low redshift could be the progenitors of massive E+A galaxies like those found in our sample.

We have performed a comprehensive study of the characteristics of the quenching that truncates the starburst in E+A galaxies. In particular, we have studied how the quenching efficiency varies as a function of galaxy mass and compared the results to scenarios where the quenching is due to SN and AGN, which are the typical sources of kinetic and thermal feedback invoked in galaxy formation models. We have found that in E+A galaxies with masses lesser than $10^{10} M_{\odot}$, quenching becomes less efficient as the galaxy mass increases. However, in galaxies with masses greater than $10^{10} M_{\odot}$, this trend is reversed and the quenching efficiency scales positively with galaxy mass. In terms of $M(z)$ and stellar velocity dispersion (σ), the reversal occurs at $M(z) \sim -21$ and $\sigma \sim 100 \text{ km s}^{-1}$.

Since the mass threshold ($10^{10} M_{\odot}$) where this reversal occurs is in excellent agreement with the mass above which AGN become significantly more abundant in nearby galaxies, these results can be qualitatively explained in terms of AGN and SN being the principal sources of feedback that quenches star formation in E+A galaxies above and below $M \sim 10^{10} M_{\odot}$ respectively. In the absence of AGN ($M < 10^{10} M_{\odot}$), the primary source of negative feedback are SN. As galaxies become more massive, the increasing depth of the potential well makes it more difficult to eject gas from the system, reducing the quenching efficiency. As a result, the quenching efficiency shows a negative correlation with galaxy mass. We have shown that simple energetic arguments, based on the assumption that quenching occurs through mechanical ejection of gas, are able to satisfy the observed properties of E+A galaxies with masses below $10^{10} M_{\odot}$. This indicates that, in these galaxies, the quenching is likely to be driven *purely* through mechanical feedback from SN.

Once they begin to appear ($M > 10^{10} M_{\odot}$), AGN be-

come the dominant source of energetic feedback. Given that the AGN luminosity scales with the mass of the black hole (M_{BH}) which, in turn, scales strongly with the central velocity dispersion σ as $M_{BH} \sim \sigma^{4-5}$, we expect AGN feedback to become more effective (and hence the quenching efficiency to increase) as the galaxy mass increases. We have shown that simple energetic arguments, based on the mechanical ejection of gas, indeed expect a positive correlation between the quenching efficiency and galaxy mass. However, the derived properties suggest that the quenching efficiencies rise an order of magnitude faster with galaxy mass than predicted by simple energetic arguments *that assume that the Eddington ratio does not vary as a function of host galaxy mass*. However, the correlation between quenching efficiency and galaxy mass can be reproduced if the Eddington ratio (μ) of the E+A galaxies is assumed to vary with M as M^{γ} , where $1 < \gamma < 3$. Since the E+A masses are spread over an order of magnitude, this implies that the Eddington ratios of the smallest AGN (with host galaxy masses $M \sim 10^{10} M_{\odot}$) are roughly one-tenth of those for their most massive counterparts in this sample (if $\gamma \sim 1$).

Finally, we have used our E+A sample to estimate the time it takes for galaxies to migrate from the blue cloud to red sequence. The persistent bimodality in galaxy colours over a large range in redshift coupled with the build-up of the red sequence over time suggests that the net migration of galaxies from the blue cloud to the red sequence is an important feature of the macroscopic evolution of the galaxy population over time. The use of E+A galaxies, which have just truncated their star formation and are on the verge of this migratory transition, together with the use of both *UV* and optical photometry, produces reasonably robust estimates of the migration times. The migration times are estimated by ‘ageing’ the best-fit SEDs of each E+A galaxy, keeping secondary parameters such as metallicity and $E(B - V)$ constant throughout the migration. We calculate migration times between 1 and 5 Gyrs, with a typical migration time of ~ 1.5 Gyrs.

The study of E+A galaxies arguably holds the key to understanding many of the processes that shape the evolution of galaxies. While our analysis is phenomenological in nature, this study has attempted to derive quantitative insights into some of these processes, especially the characteristics of feedback that is responsible for modulating and truncating star formation in galaxies. While many of the results derived here (e.g. timescales over which AGN or SN feedback quenches star formation, the comparative efficiencies of the two feedback modes in potential wells of varying sizes or the migration times from the blue cloud to the red sequence) could prove useful constraints in galaxy formation models, future studies of E+A galaxies at high redshift are keenly anticipated because they will provide key insights into how such processes, that dictate the evolution of the galaxy population, evolve over time.

ACKNOWLEDGEMENTS

We are grateful to the anonymous referee for numerous insightful comments that improved the clarity of the original manuscript. The work presented in this paper would not have been possible without the Garching SDSS catalog. SK

is grateful to Christy Tremonti for many useful discussions regarding the extraction of spectroscopic parameters used in this study. Sven De Rijcke, James Binney, Lisa Young, Phillip Podsiadlowski and Sukyoung Yi are thanked for constructive comments.

SK acknowledges a Leverhulme Early-Career Fellowship, a BIPAC Fellowship and a Research Fellowship from Worcester College, Oxford. Part of the research presented in this study used the undergraduate computing facilities in the Department of Physics at Oxford.

Funding for the SDSS and SDSS-II has been provided by the Alfred P. Sloan Foundation, the Participating Institutions, the National Science Foundation, the U.S. Department of Energy, the National Aeronautics and Space Administration, the Japanese Monbukagakusho, the Max Planck Society, and the Higher Education Funding Council for England. The SDSS Web Site is <http://www.sdss.org/>.

The SDSS is managed by the Astrophysical Research Consortium for the Participating Institutions. The Participating Institutions are the American Museum of Natural History, Astrophysical Institute Potsdam, University of Basel, University of Cambridge, Case Western Reserve University, University of Chicago, Drexel University, Fermilab, the Institute for Advanced Study, the Japan Participation Group, Johns Hopkins University, the Joint Institute for Nuclear Astrophysics, the Kavli Institute for Particle Astrophysics and Cosmology, the Korean Scientist Group, the Chinese Academy of Sciences (LAMOST), Los Alamos National Laboratory, the Max-Planck-Institute for Astronomy (MPIA), the Max-Planck-Institute for Astrophysics (MPA), New Mexico State University, Ohio State University, University of Pittsburgh, University of Portsmouth, Princeton University, the United States Naval Observatory, and the University of Washington.

REFERENCES

- Bekki K., Shioya Y., Couch W. J., 2001, *ApJ*, 547, L17
- Bell E. F., Wolf C., Meisenheimer K., Rix H.-W., Borch A., Dye S., Kleinheinrich M., Wisotzki L., McIntosh D. H., 2004, *ApJ*, 608, 752
- Belloni P., Bruzual A. G., Thimm G. J., Roser H.-J., 1995, *A&A*, 297, 61
- Bernardi M., the SDSS collaboration 2003, *AJ*, 125, 1882
- Blake C., 2dF collaboration 2004, *MNRAS*, 355, 713
- Bondi H., Hoyle F., 1944, *MNRAS*, 104, 273
- Bower R. G., Lucey J. R., Ellis R., 1992, *MNRAS*, 254, 589
- Bressan A., Poggianti B., Franceschini A., 2001, in Márquez I., Masegosa J., del Olmo A., Lara L., García E., Molina J., eds, *QSO Hosts and Their Environments* pp 171–+
- Brinchmann J., Charlot S., White S. D. M., Tremonti C., Kauffmann G., Heckman T., Brinkmann J., 2004, *MNRAS*, 351, 1151
- Buyle P., Michielsen D., De Rijcke S., Pisano D. J., Dejonghe H., Freeman K., 2006, *ApJ*, 649, 163
- Chang T.-C., van Gorkom J. H., Zabludoff A. I., Zaritsky D., Mihos J. C., 2001, *AJ*, 121, 1965
- Couch W. J., Sharples R. M., 1987, *MNRAS*, 229, 423
- Cowie L. L., Songaila A., Hu E. M., Cohen J. G., 1996, *AJ*, 112, 839
- Dressler A., Gunn J. E., 1983, *ApJ*, 270, 7
- Fabricant D. G., McClintock J. E., Bautz M. W., 1991, *ApJ*, 381, 33
- Ferrarese L., Merritt D., 2000, *ApJ*, 539, L9
- Fukugita M., Hogan C. J., Peebles P. J. E., 1998, *ApJ*, 503, 518
- Galaz G., 2000, *AJ*, 119, 2118
- Gebhardt K., Bender R., Bower G., Dressler A., Faber S. M., Filippenko A. V., Green R., Grillmair C., Ho L. C., Kormendy J., Lauer T. R., Magorrian J., Pinkney J., Richstone D., Tremaine S., 2000, *ApJ*, 539, L13
- Goto T., 2004, *A&A*, 427, 125
- Goto T., 2005, *MNRAS*, 357, 937
- Goto T., 2006, *MNRAS*, 369, 1765
- Goto T., SDSS collaboration 2003, *PASJ*, 55, 771
- Håring N., Rix H.-W., 2004, *ApJ*, 604, L89
- Kauffmann G., Heckman T. M., Tremonti C., Brinchmann J., Charlot S., White S. D. M., Ridgway S. E., Brinkmann J., Fukugita M., Hall P. B., Ivezić Ž., Richards G. T., Schneider D. P., 2003a, *MNRAS*, 346, 1055
- Kauffmann G., SDSS collaboration 2003b, *MNRAS*, 341, 33
- Kaviraj S., Devriendt J. E. G., Ferreras I., Yi S. K., Silk J., 2006b, Submitted to *MNRAS*, astro-ph/0602347
- Kaviraj S., GALEX Science Team 2006a, Accepted for publication in *ApJ*, to appear in GALEX dedicated issue in December 2007, astro-ph/0601029
- Kaviraj S., Rey S., Rich R. M., Lee Y., Yoon S., Yi S. K., 2007, *MNRAS* in press, astro-ph/0601050
- Kennicutt Jr. R. C., 1998, *ApJ*, 498, 541
- Liu C. T., Green R. F., 1996, *ApJ*, 458, L63+
- Liu C. T., Hooper E. J., O’Neil K., Thompson D., Wolf M., Lisker T., 2007, *ApJ*, 658, 249
- Martin D. C., GALEX collaboration 2005, *ApJ*, 619, L1
- Mihos J. C., Hernquist L., 1994, *ApJ*, 437, L47
- Miller N. A., Owen F. N., 2001, *ApJ*, 554, L25
- Norton S. A., Gebhardt K., Zabludoff A. I., Zaritsky D., 2001, *ApJ*, 557, 150
- Poggianti B. M., Bressan A., Franceschini A., 2001, *ApJ*, 550, 195
- Poggianti B. M., Wu H., 2000, *ApJ*, 529, 157
- Quintero A. D., Hogg D. W., Blanton M. R., Schlegel D. J., Eisenstein D. J., Gunn J. E., Brinkmann J., Fukugita M., Glazebrook K., Goto T., 2004, *ApJ*, 602, 190
- Sanders D. B., Mirabel I. F., 1996, *A&RAA*, 34, 749
- Shankar F., Lapi A., Salucci P., De Zotti G., Danese L., 2006, *ApJ*, 643, 14
- Smail I., Morrison G., Gray M. E., Owen F. N., Ivison R. J., Kneib J.-P., Ellis R. S., 1999, *ApJ*, 525, 609
- Tran K.-V. H., Franx M., Illingworth G. D., van Dokkum P., Kelson D. D., Magee D., 2004, *ApJ*, 609, 683
- Tremonti C. A., Heckman T. M., Kauffmann G., Brinchmann J., Charlot S., White S. D. M., Seibert M., Peng E. W., Schlegel D. J., Uomoto A., Fukugita M., Brinkmann J., 2004, *ApJ*, 613, 898
- Wang J. L., Xia X. Y., Mao S., Cao C., Wu H., Deng Z. G., 2006, *ApJ*, 649, 722
- Yang Y., Zabludoff A. I., Zaritsky D., Lauer T. R., Mihos J. C., 2004, *ApJ*, 607, 258
- Yi S. K., 2003, *ApJ*, 582, 202
- Yi S. K., GALEX Science Team 2005, *ApJ*, 619, L111
- Zabludoff A. I., Zaritsky D., Lin H., Tucker D., Hashimoto Y., Shectman S. A., Oemler A., Kirshner R. P., 1996, *ApJ*,

